Annals of Glaciology

Supplementary material for

A framework for attenuation method selection evaluated with ice-penetrating radar data at South Pole Lake

Benjamin H. Hills[1,2], Knut Christianson[1], Nicholas Holschuh[1,3]

[1]*Department of Earth and Space Sciences, University of Washington, Seattle, WA, USA*
[2]*Polar Science Center, Applied Physics Laboratory, University of Washington, Seattle, WA, USA*
[3]*Department of Geology, Amherst College, Amherst, MA, USA*

Contents of this file

Text S1

Figures S1 to S7

S1. Interval versus depth-averaged attenuation rate

Throughout the manuscript, we refer to single-reflector attenuation rates as an interval result (e.g. Fig. 3), implying that they are representative of only the ice which the reflector spans. Prior studies generally have discussed single-reflector attenuation rates as a depth-averaged result, representing all ice above the reflector (ice through which the radio wave travels) (Jacobel et al., 2009; Schroeder et al., 2016). Here, we argue that under the implied assumptions for single-reflector methods (i.e. that $\left|\frac{\partial[R]}{\partial z}\right| \ll \left|\frac{\partial[P_c]}{\partial z}\right|$ and that $\left|\frac{\partial N}{\partial x}\right| \ll 0$), the only well-posed problem is that of pure conduction. In this well-posed case, attenuative losses above the shallowest reflection are spatially uniform, and the regression is *exactly* equal to the interval attenuation rate over the depth range which the reflector spans. In any more realistic case, vertical and horizontal advection as well as heat generation create horizontal temperature gradients in the ice which violate the assumptions, creating an ill-posed problem, and possibly bias the calculated attenuation rate. Having said that, the bias is not necessarily toward the depth-averaged value, the direction of the bias depends on the direction of the temperature gradient.
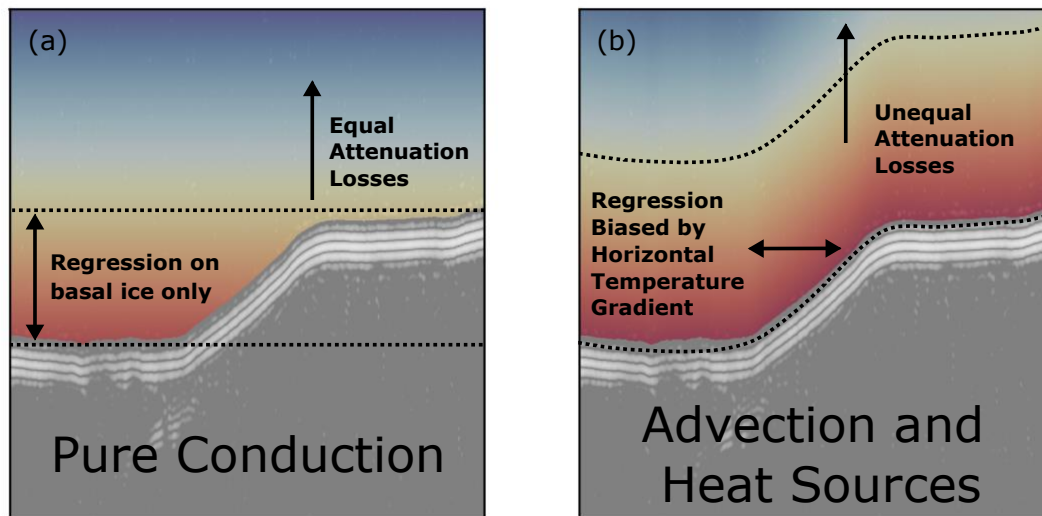

Figure S1. *A thought experiment for single-reflector attenuation calculations under two scenarios. In each, the temperature-dependent instantaneous attenuation rate (colormap) is overlain on a portion of the bed reflector from the radar image in Figure 1. a) Pure conduction controls the ice temperature while the surface temperature and geothermal flux are uniform. In this scenario, there is no horizontal temperature gradient, so temperature-related attenuative losses are identical between traces, and the depth-power regression on the bed reflector represents characteristics of the basal ice only (i.e. between the dotted lines). b) Additional heat transfer processes create a horizontal temperature gradient which can bias the regression in either direction (toward or away from the depth-averaged attenuation rate).*

In order to illustrate this problem more quantitatively, we create a synthetic glacier profile and calculate synthetic attenuation rates below. The examples are not designed to precisely model any 'real' glaciological setting, but are intended to demonstrate the various possible biases in single-reflector attenuation calculations. We define the glacier thickness profile using the Vialov equation (Cuffey and Paterson, 2010 equation 8.138). This equation assumes no sliding, a flat bed, a constant flow-band width, constant accumulation of 10 cm/yr, and a constant rate factor, $A=3.5*10^{-25}$ s^{-1} Pa^{-3}. Ice temperature is defined using a 1-dimensional analytical solution that allows nonlinear vertical velocity (Rezvanbehbahani et al., 2019). For each trace, we optimize the exponent on the vertical velocity profile based on a logarithmic regression with the Peclet Number (Rezvanbehbahani et al., 2019 section 2.3). Heat production associated with xz-strain in the column is added by increasing the geothermal flux term (Rezvanbehbahani et al., 2019 section 3). For the final case, we switch the temperature model to an alternative analytical solution which more appropriately represents a setting with strong xy-strain heat generation and a significant thicknesses of temperate ice (Meyer and Minchew, 2018).

The instantaneous attenuation rate is calculated at all depths of the temperature profile using a temperature- and chemistry-dependent Arrhenius model (MacGregor et al., 2007). We use constant acidity (1.3 μM H_+) and constant sea salts (4.2 μM ss Cl_-). For each trace, we integrate the instantaneous attenuation rate over the ice column to calculate the power losses at the bed. Then, the *Method 1* attenuation rate is calculated at the bed reflector using the EIV regression (Appendix).

In the case of pure conduction (Fig. S2), the single-reflector attenuation rate is *exactly* equal to the interval attenuation rate. Adding a constant accumulation (Fig. S3) biases the result lower (i.e. toward the depth-averaged result). Adding heat production from xz-shear (Fig. S4) biases the result high, bringing it back toward the interval rate. In the case where we define air temperature and accumulation with a lapse rate (Fig. S5), the attenuation rate is biased lower than even the depth-averaged value. When we impose a linear gradient in the geothermal flux, increasing toward the ice divide (Fig. S6), the attenuation rate is biased slightly high. Finally, switching to the temperate-ice model biases the result very high until the basal ice is temperate, then the result exactly represents that of the interval attenuation rate.

For all cases, the single-reflector attenuation rate is only biased away from the interval value when the ice has a horizontal temperature gradient with respect to the cold surface boundary. The strongest horizontal gradients arise when there is some variation in heat production (e.g. near an ice stream shear margin (Holschuh et al., 2019)). However, more subtle gradients arise in almost any setting (Hills et al., 2017). For example, in the case of a spatially uniform accumulation rate (with the vertical velocity varying only in the vertical) thickness variations create a subtle horizontal temperature gradient (Fig. S3). Unfortunately though, it is difficult to know exactly which way the single-reflector attenuation rate calculation will be biased without knowing the ice temperature, and in that case the attenuation could be modeled confidently.
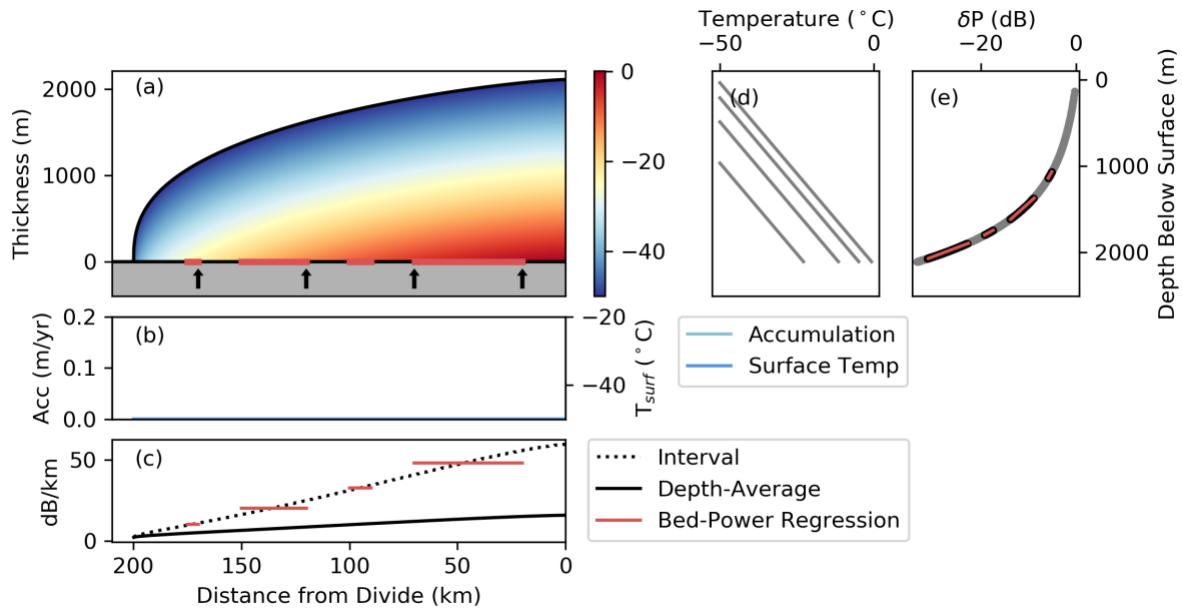
Figure S2. *Synthetic attenuation calculations using Method 1 (bed reflector). For this case, the accumulation rate is zero, the air temperature is constant (-50°C), and the geothermal flux is constant (50 mW/m2). a) Glacier thickness profile with the colormap showing ice temperature, grey is bedrock. The arrows show locations where temperature profiles are plotted in (d). The red sections along the bed reflector are where attenuation is calculated and correspond to red lines in (c) and (e). b) Accumulation and air temperature profiles. c) Attenuation profiles where the solid line is averaged over the ice thickness, the dotted line is the instantaneous value at the bed, and the red lines are regressions. d) Temperature profiles corresponding to arrow locations in (a). e) The power differential at the bed reflector associated with attenuative losses through the column.*
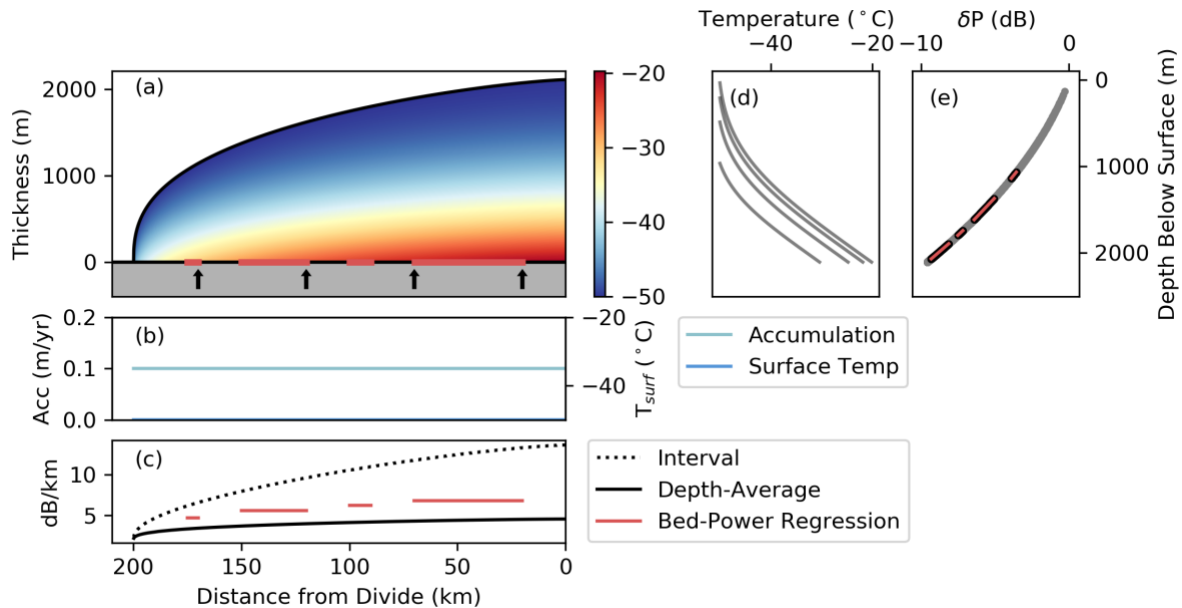

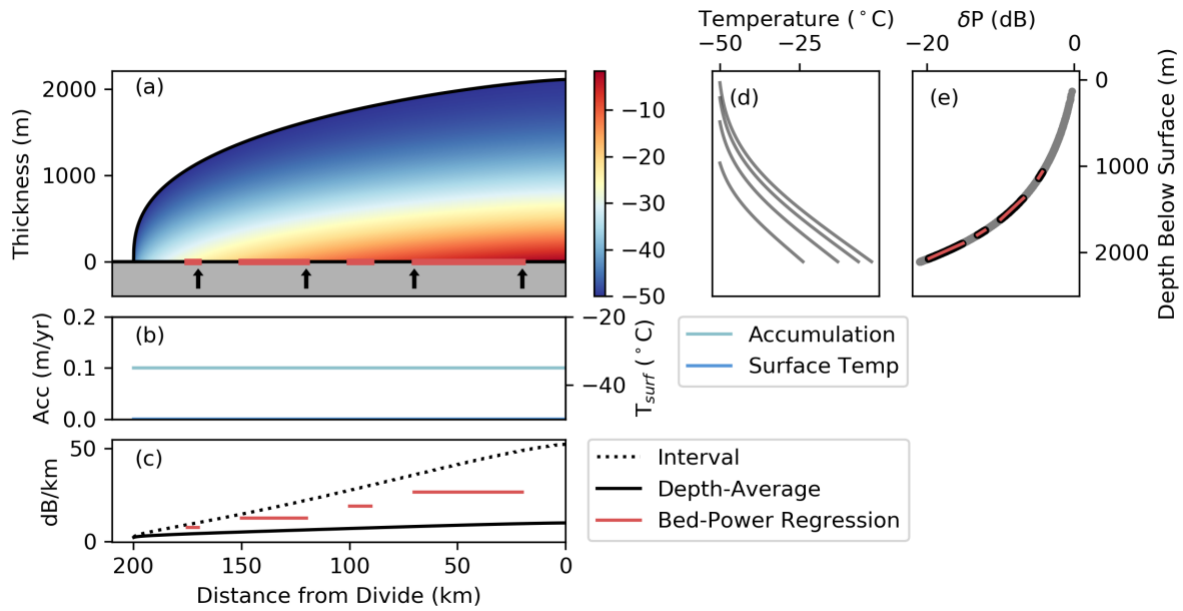**Figure S3.** *Same as S1 but with uniform non-zero accumulation (10 cm/yr).*

Figure S4. *Same as S1 but with uniform non-zero accumulation (10 cm/yr) and heat production from xz-shear strain (100kPa).*
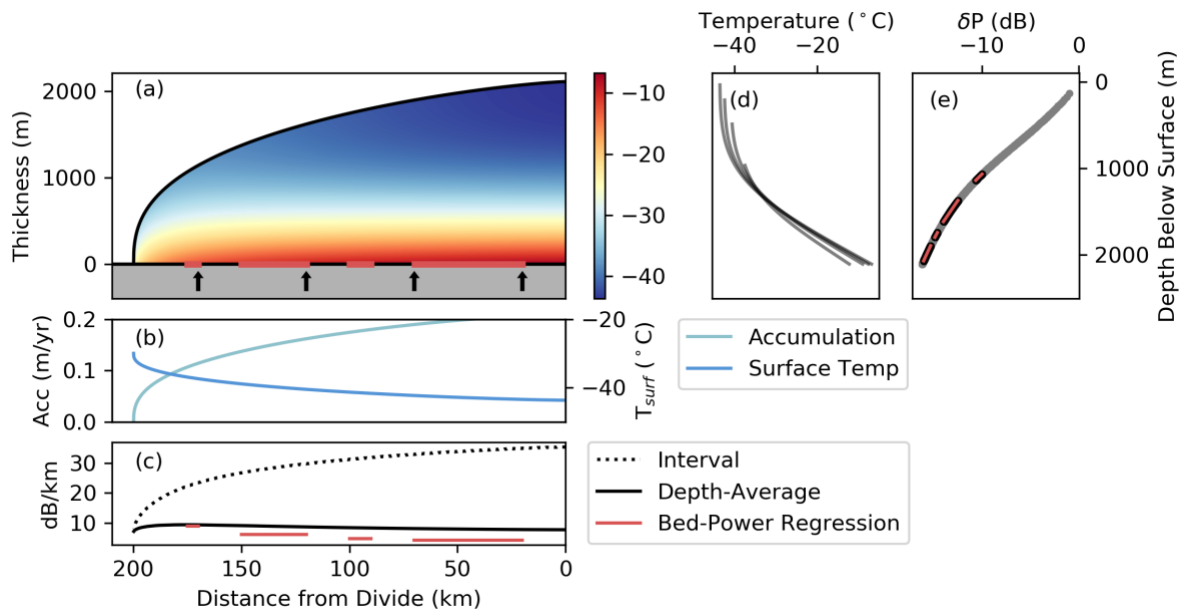

Figure S5. *Same as S1 but with accumulation and air temperature defined by the thickness profile. Accumulation is zero at the ice margin and increasing by 10 cm/yr per 1 km elevation. Air temperature is -30°C at the ice margin and decreasing by 6.5°C per 1 km elevation.*
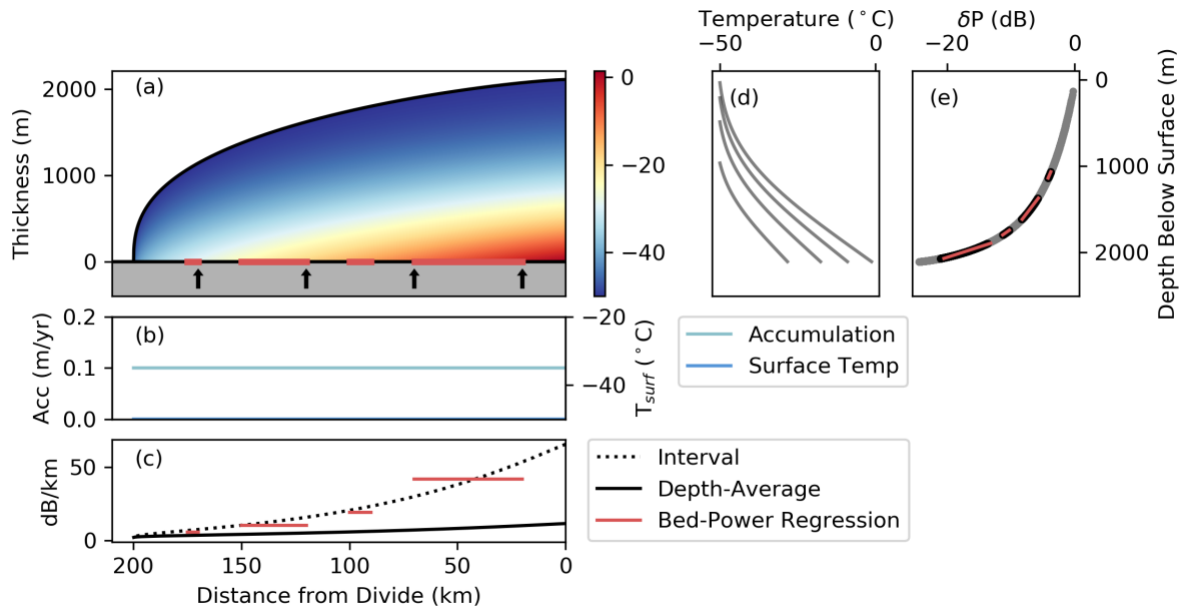
Figure S6. *Same as S1 but with uniform non-zero accumulation (10 cm/yr) and geothermal flux increasing linearly from 50 mW/m2 at the glacier margin to 85 mW/m2 at the ice divide.*
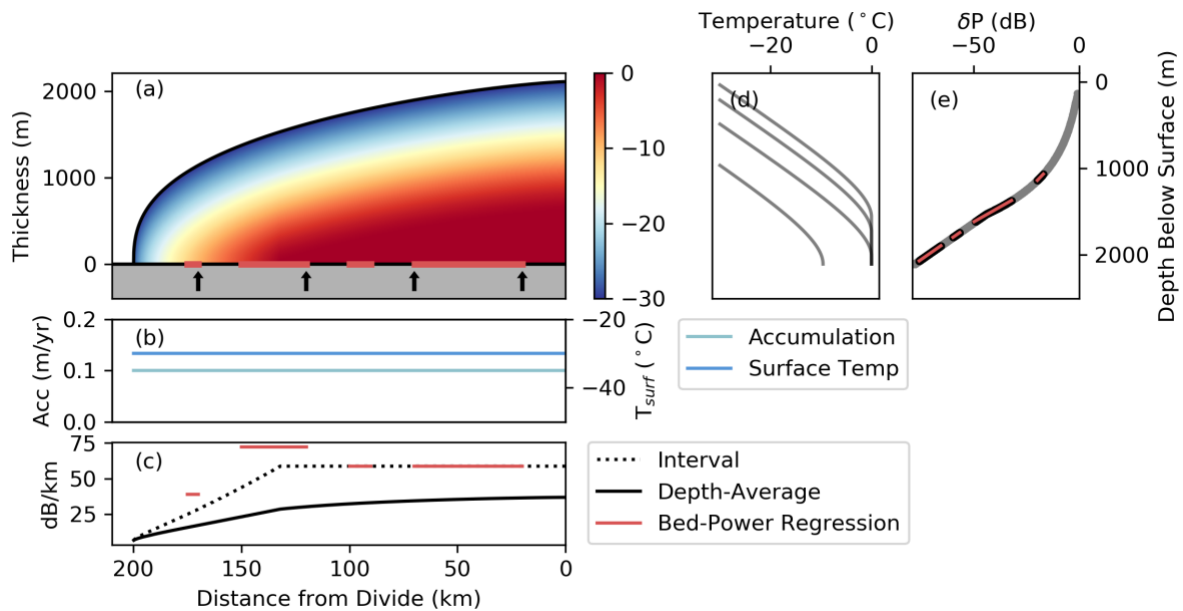

Figure S7. *Same as S1 but uniform non-zero accumulation (10 cm/yr), warmer air temperature (-30°C), a strong heat source from xy-shear strain (.02 yr-1), and with the temperature profile defined by an alternative analytical solution more appropriate for temperate ice (Meyer and Minchew, 2018).*

References

Cuffey, K., Paterson, W.S.B., 2010. The Physics of Glaciers, Fourth. ed. Butterworth-Heinemann, Oxford, UK.

Hills, B.H., Harper, J.T., Humphrey, N.F., Meierbachtol, T.W., 2017. Measured horizontal temperature gradients constrain heat transfer mechanisms in Greenland ice. Geophys. Res. Lett. 44. https://doi.org/10.1002/2017GL074917

Holschuh, N., Lilien, D.A., Christianson, K., 2019. Thermal Weakening, Convergent Flow, and Vertical Heat Transport in the Northeast Greenland Ice Stream Shear Margins. Geophys. Res. Lett. 8184–8193. https://doi.org/10.1029/2019gl083436

Jacobel, R.W., Welch, B.C., Osterhouse, D., Pettersson, R., Macgregor, J.A., 2009. Spatial variation of radar-derived basal conditions on Kamb Ice Stream, West Antarctica. Ann. Glaciol. 50, 10–16. https://doi.org/10.3189/172756409789097504

MacGregor, J.A., Winebrenner, D.P., Conway, H., Matsuoka, K., Mayewski, P.A., Clow, G.D., 2007. Modeling englacial radar attenuation at Siple Dome, West Antarctica, using ice chemistry and temperature data. J. Geophys. Res. Earth Surf. 112, 1–14. https://doi.org/10.1029/2006JF000717

Meyer, C.R., Minchew, B.M., 2018. Temperate ice in the shear margins of the Antarctic Ice Sheet: Controlling processes and preliminary locations. Earth Planet. Sci. Lett. 498, 17–26. https://doi.org/10.1016/j.epsl.2018.06.028

Rezvanbehbahani, S., van der Veen, C.J., Stearns, L.A., 2019. An Improved Analytical Solution for the Temperature Profile of Ice Sheets. J. Geophys. Res. Earth Surf. 124, 271–286. https://doi.org/10.1029/2018JF004774

Schroeder, D.M., Seroussi, H., Chu, W., Young, D.A., 2016. Adaptively constraining radar attenuation and temperature across the Thwaites Glacier catchment using bed echoes. J. Glaciol. 62, 1075–1082. https://doi.org/10.1017/jog.2016.100